Supplemental Material:
Transient Valence Charge Localization in Strong-Field Dissociative Ionization of HCl Molecules

Junyang Ma,[1,2] Liang Xu,[3,4] Hongcheng Ni,[1,5] Chenxu Lu,[1] Wenbin Zhang,[1]
Peifen Lu,[1] Jin Wen,[6] Feng He,[3,7] Olivier Faucher,[2] and Jian Wu[1,5,7]

[1]*State Key Laboratory of Precision Spectroscopy, East China Normal University, Shanghai 200241, China*
[2]*Laboratoire Interdisciplinaire CARNOT de Bourgogne,*
UMR 6303 CNRS-Université Bourgogne Franche-Comté, BP 47870, 21078 Dijon, France
[3]*Key Laboratory for Laser Plasmas (Ministry of Education) and School of Physics and Astronomy,*
Collaborative Innovation Center for IFSA (CICIFSA), Shanghai Jiao Tong University, Shanghai 200240, China
[4]*Shanghai Key Lab of Modern Optical System, University of Shanghai for Science and Technology, Shanghai 200093, China*
[5]*Collaborative Innovation Center of Extreme Optics, Shanxi University, Taiyuan, Shanxi 030006, China*
[6]*State Key Laboratory for Modification of Chemical Fibers and Polymer Materials and*
College of Materials Science and Engineering, Donghua University, Shanghai 201620, China
[7]*CAS Center for Excellence in Ultra-intense Laser Science, Shanghai 201800, China*

CROSSCHECK WITH LEFT- AND RIGHT-HANDED ELLIPTICAL POLARIZATIONS

Our experimental results are crosschecked with LEP and REP (left- and right-handed elliptical polarizations), as shown in Fig. S1, allowing us to rule out systematical errors. Fig. S1(a) is the same as Fig. 3 of the main text employing LEP, and REP pulse is employed to produce Fig. S1(b). It is clear that the same conclusion holds for LEP and REP.

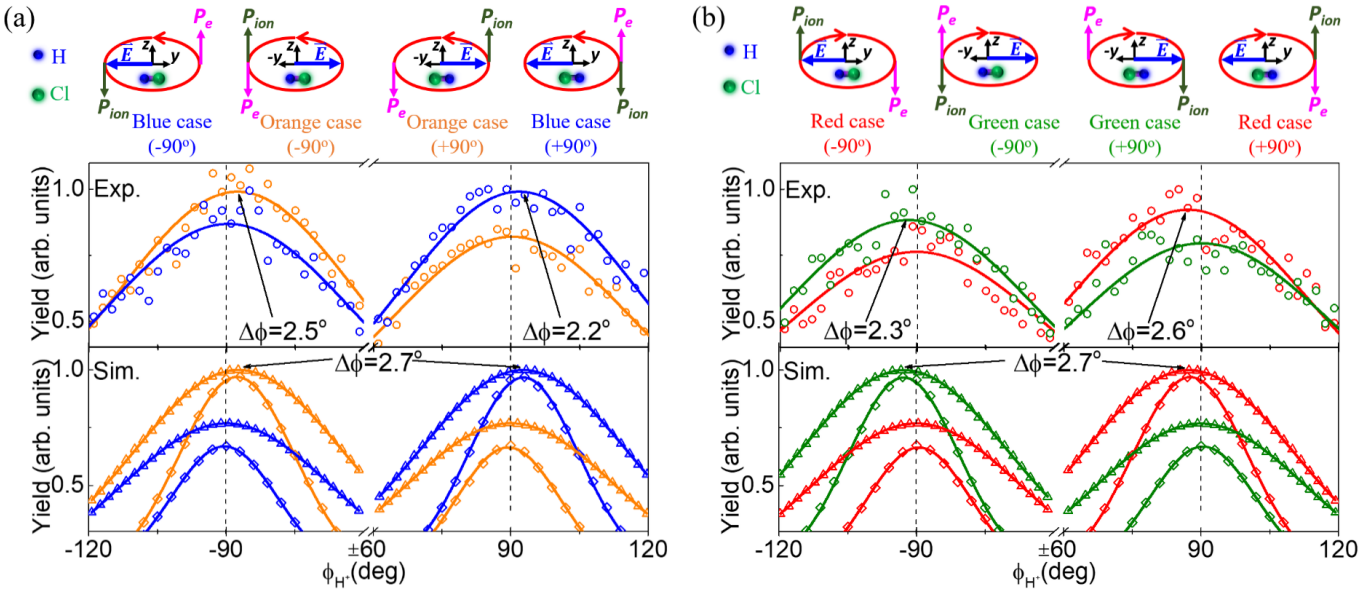

FIG. S1. (a) The open circles (fitted with solid curves) are the measured angular distributions of the H^+ fragments of the HCl(1, 0) channel when the electron is released from two different sites driven by the LEP field as illustrated in the individual sketches. The black dashed lines represent the positions of $\pm 90°$. $\Delta\phi$ is the offset angle of the peak position of the fitted curves with respect to the y axis ($\pm 90°$). The open triangles and diamonds (fitted with solid curves) are the corresponding classical and quantum simulation results, respectively. (b) Same as (a) but for REP.

QUANTUM DYNAMICS SIMULATIONS OF THE FRAGMENTATION PROCESS

We employ a two-level quantum dynamics simulations of the fragmentation process. To enable the simulations of the rotation dynamics, we use a two-dimensional model, where the nuclear dynamics is restricted on the $y-z$ plane. As shown before [1], the dissociation process of HCl process involves mainly the $A^2\Sigma^+$ and $2^2\Sigma^+$ states, which are thus used in the two-level quantum simulations. The following two-level time-dependent Schrödinger equation (TDSE) is solved with origin at the center of mass

of the nuclei (in atomic units) [2]:

$$i\frac{\partial}{\partial t}\begin{pmatrix}\chi_1(\boldsymbol{R},t)\\ \chi_2(\boldsymbol{R},t)\end{pmatrix}=\begin{pmatrix}H_1(\boldsymbol{R},t) & \boldsymbol{\mu}_{12}(\boldsymbol{R})\cdot\boldsymbol{E}(t)\\ \boldsymbol{\mu}_{12}(\boldsymbol{R})\cdot\boldsymbol{E}(t) & H_2(\boldsymbol{R},t)\end{pmatrix}\begin{pmatrix}\chi_1(\boldsymbol{R},t)\\ \chi_2(\boldsymbol{R},t)\end{pmatrix}, \tag{S1}$$

where the subscripts 1 and 2 represent the variables related to the $A^2\Sigma^+$ and $2^2\Sigma^+$ states, respectively, $\chi(\boldsymbol{R},t)$ is the HCl^+ nuclear wave packet, $\boldsymbol{R}$ is the internuclear distance vector, $\boldsymbol{E}(t)$ is the laser electric field vector, $\boldsymbol{\mu}_{12}(\boldsymbol{R})$ is the transition dipole moment between the $A^2\Sigma^+$ and $2^2\Sigma^+$ states, and $H_{1/2}(\boldsymbol{R},t)=p_R^2/2M+V_{1/2}(\boldsymbol{R})-\boldsymbol{\mu}_{1/2}(\boldsymbol{R})\cdot\boldsymbol{E}(t)-\boldsymbol{E}(t)\boldsymbol{\alpha}_{1/2}(\boldsymbol{R})\boldsymbol{E}(t)/2$, where p_R is the momentum and M is the mass of the reduced nucleus, $V_{1/2}(\boldsymbol{R})$ is the potential energy curve of the $A^2\Sigma^+$ and $2^2\Sigma^+$ states, and $\boldsymbol{\mu}_{1/2}(\boldsymbol{R})$ and $\boldsymbol{\alpha}_{1/2}$ is their respective permanent dipole moment and polarizability tensor.

To prepare the initial state of the nuclear wave packet, we solve the following TDSE for the ground state of HCl nuclear wave packet $\chi_0(\boldsymbol{R},t)$:

$$i\frac{\partial}{\partial t}\chi_0(\boldsymbol{R},t)=\left[\frac{p_R^2}{2M}+V_0(\boldsymbol{R})\right]\chi_0(\boldsymbol{R},t), \tag{S2}$$

where $V_0(\boldsymbol{R})$ is the potential energy curve of the $X^1\Sigma^+$ ground state of the HCl molecule. During each time step within a laser optical cycle, the $X^1\Sigma^+$ ground state $\chi_0(\boldsymbol{R},t)$ is brought vertically via Frank-Condon transition to the $A^2\Sigma^+$ and $2^2\Sigma^+$ states, with $\chi_{1/2}(\boldsymbol{R},t)=\chi_0(\boldsymbol{R},t)g_{1/2}(\boldsymbol{R},t)w_{1/2}(\boldsymbol{R},t)$, where $g_{1/2}(\boldsymbol{R},t)$ is the structure factor accounting for the shape of the ionizing molecular orbital (HOMO-1 corresponding to populated $A^2\Sigma^+$ state and HOMO-2 populated $2^2\Sigma^+$ state, see Fig. S2) [3, 4] and $w_{1/2}(\boldsymbol{R},t)=\exp\{-[2\tilde{I}_p(\boldsymbol{R},t)]^{3/2}/3E(t)\}$ is the field factor accounting for the ionization rate, where $\tilde{I}_p(\boldsymbol{R},t)$ is the effective ionization potential with $\tilde{I}_p(\boldsymbol{R},t)=V_{1/2}(\boldsymbol{R})-V_0(\boldsymbol{R})-[\boldsymbol{\mu}_{1/2}(\boldsymbol{R})-\boldsymbol{\mu}_0(\boldsymbol{R})]\cdot\boldsymbol{E}(t)-\boldsymbol{E}(t)[\boldsymbol{\alpha}_{1/2}(\boldsymbol{R})-\boldsymbol{\alpha}_0(\boldsymbol{R})]\boldsymbol{E}(t)/2$. We note that this form of the ionization rate is in line with the weak-field asymptotic theory (WFAT) for polar molecules [5] by Taylor expansion in terms of the dipole moment.

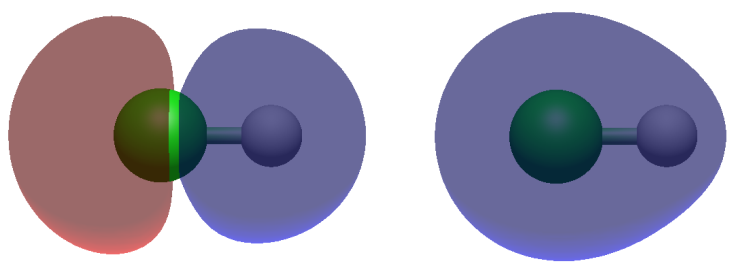

FIG. S2. The HOMO-1 (left) and HOMO-2 (right) molecular orbitals of the HCl molecule.

In the present two-level quantum model, the asymmetric charge distribution is caused by different population on the $A^2\Sigma^+$ and $2^2\Sigma^+$ states, which arises from the heteronuclear nature of the HCl molecule. The heteronuclear nature of the molecule has two consequences: (1) there is a permanent dipole in the molecule; (2) the shape of the molecular orbital is asymmetric, leading to different electron density near different nuclei. In the following, let us consider the effect of each of these two factors.

We first consider the effect of the permanent dipole moment. The dissociation limit of the $A^2\Sigma^+$ state is H^+ and Cl, so the dipole of this state points from Cl to H; conversely, the dipole of the $2^2\Sigma^+$ state points from H to Cl. Consequently, when the laser electric field points from H to Cl and the electron tunnels from H side, the energy of the $A^2\Sigma^+$ state gets higher while that of the $2^2\Sigma^+$ state gets lower. Due to such energy shift, there is less positive charge on H, and less H^+ are produced, when the electric field points from H to Cl, as compared to the case when the field points from Cl to H. Obviously, such effect from the permanent dipole contradicts our experimental observations.

Now we consider the effect of the molecular orbital shape, which is reflected in the molecular structure factor [3–5]. The $A^2\Sigma^+$ ionic state is populated when the HOMO-1 electron is removed from the neutral HCl molecule, and the $2^2\Sigma^+$ state is populated by removal of the HOMO-2 electron. It is clear from Fig. S2 that the electron density is higher on the H side for HOMO-1 and the electron density is higher on the Cl side for HOMO-2. Consequently, when the laser electric field points from H to Cl and the electron tunnels from H side, the $A^2\Sigma^+$ state would have more population and the $2^2\Sigma^+$ state would have less population, as compared to the opposite case when the field points from Cl to H. Therefore, when the laser electric field points from H to Cl, there will be more H^+ generated and there would be more positive charge on H, in agreement with our experiments.

As a matter of fact, the opposite effect of the permanent dipole to the experiments has been observed for a variety of molecules [7, 8]. It has been concluded that the effect of the molecular orbital shape often outweighs the effect of the permanent dipole. That said, we note that for the extremely asymmetric molecule such as HeH^+, the permanent dipole plays a crucial role [9, 10].

On the technical front, the molecular structure factor, potential energy curve, dipole moment, and polarizability tensor for different electronic states are calculated with the complete active space self-consistent field method (CASSCF) using the PySCF package [6]. For HCl^+, the active space includes 7 electrons and 11 orbitals, corresponding to the Cl $3s3p3d$ and H $1s2s2p$ shells, with the Cl d_{z^2}, $d_{x^2-y^2}$, d_{xy} shells excluded from the active space. The dipole moment $\boldsymbol{\mu}$ and polarizability tensor $\boldsymbol{\alpha}$ are calculated by adding a weak perturbative field along ($F_\parallel$) or perpendicular ($F_\perp$) to the molecular bond direction and reconstructed from the energy level shiftings [11]:

$$\mu = (E(-F_\parallel) - E(F_\parallel))/(2F_\parallel), \tag{S3}$$

$$\alpha_\parallel = (2E(0) - E(-F_\parallel) - E(F_\parallel))/F_\parallel^2, \tag{S4}$$

$$\alpha_\perp = 2(E(0) - E(F_\perp))/F_\perp^2. \tag{S5}$$

To emulate a static perturbative field, we add two point charges with charge $+50$ and -50 at a distance of $+200$ or -200 from the origin, which forms a near-uniform static field at the origin and produces the desired energy level shiftings.

To obtain the angular distribution of the ejected proton, we study the nuclear wave packet on the $A^2\Sigma^+$ state, whose dissociation products are H^+ and Cl, after the laser pulse is over. To obtain the dissociated part of the nuclear wave packet, we drop out the nuclear wave function for $R < 4.5$ a.u. To study the angular distribution of the proton on the subcycle level, we separate the cases when the field points from Cl to H and from H to Cl.

CLASSICAL DYNAMICS SIMULATIONS OF THE FRAGMENTATION PROCESS

For the sake of a clear physical picture, we additionally carry out a classical dynamics simulation of the fragmentation process incorporating a localized transient charge on the respective fragments. In principle, the electron or charge cloud is always a broad distribution around the nucleus. For the present observable of the momentum of the ionic fragment, however, a simplified description with the charge sitting at the nucleus is plausible since the final momentum of the ion is an integrated observable with respect to its charge distribution. When the charge is shared between the two nuclei during the fragmentation process, a decomposition of the charge center onto the respective nuclei is also possible. Furthermore, the oscillation of the charge localization between the nuclei can be neglected because its period is much shorter than the laser period under equilibrium internuclear separation. With these considerations in mind, we place the center of mass of the neutral HCl molecule as well as the resulting fragments at the origin. The equations of motion of the three fragments can be written as (in atomic units)

$$\begin{cases} m_{\mathrm{H}} \frac{d\boldsymbol{r}_{\mathrm{H}}^2}{dt^2} = Z_{\mathrm{H}}(t)\boldsymbol{E}(t) - \frac{\partial U}{\partial R}\boldsymbol{e}_R - Z_{\mathrm{H}}(t)\frac{\boldsymbol{r}_{\mathrm{H}}-\boldsymbol{r}_{\mathrm{e}}}{|\boldsymbol{r}_{\mathrm{H}}-\boldsymbol{r}_{\mathrm{e}}|^3}, \\ m_{\mathrm{Cl}} \frac{d\boldsymbol{r}_{\mathrm{Cl}}^2}{dt^2} = Z_{\mathrm{Cl}}(t)\boldsymbol{E}(t) + \frac{\partial U}{\partial R}\boldsymbol{e}_R - Z_{\mathrm{Cl}}(t)\frac{\boldsymbol{r}_{\mathrm{Cl}}-\boldsymbol{r}_{\mathrm{e}}}{|\boldsymbol{r}_{\mathrm{Cl}}-\boldsymbol{r}_{\mathrm{e}}|^3}, \\ \frac{d\boldsymbol{r}_{\mathrm{e}}^2}{dt^2} = -\boldsymbol{E}(t) - Z_{\mathrm{H}}(t)\frac{\boldsymbol{r}_{\mathrm{e}}-\boldsymbol{r}_{\mathrm{H}}}{|\boldsymbol{r}_{\mathrm{e}}-\boldsymbol{r}_{\mathrm{H}}|^3} - Z_{\mathrm{Cl}}(t)\frac{\boldsymbol{r}_{\mathrm{e}}-\boldsymbol{r}_{\mathrm{Cl}}}{|\boldsymbol{r}_{\mathrm{e}}-\boldsymbol{r}_{\mathrm{Cl}}|^3}, \end{cases} \tag{S6}$$

where $\boldsymbol{r}_{\mathrm{H}}$, $\boldsymbol{r}_{\mathrm{Cl}}$, and $\boldsymbol{r}_{\mathrm{e}}$ are the position vectors of H, Cl, and the electron, respectively, $\boldsymbol{m}_{\mathrm{H}} = 1836$ a.u. is the mass of the H fragment, $\boldsymbol{m}_{\mathrm{Cl}} = 64570$ a.u. is the mass of the Cl fragment, $Z_{\mathrm{H}}(t)$ and $Z_{\mathrm{Cl}}(t)$ are the transient ionic charges on H and Cl satisfying $Z_{\mathrm{H}}(t) + Z_{\mathrm{Cl}}(t) = 1$, $\boldsymbol{E}(t)$ is the laser electric field, $\boldsymbol{R} = \boldsymbol{r}_{\mathrm{H}} - \boldsymbol{r}_{\mathrm{Cl}}$ is the internuclear distance vector with R its magnitude, $\boldsymbol{e}_R = \boldsymbol{R}/R$ is the internuclear unit vector, and $U(R)$ is the potential energy curve as displayed in Fig. 2(b) of the main text. Here, we use the field-free potential energy curve, instead of that modulated by the coupling of the permanent dipole moment to the laser electric field, because the ionic charge indeed contains the information of the dipole moment, defined as $\boldsymbol{\mu} = Z_{\mathrm{H}}\boldsymbol{r}_{\mathrm{H}} + Z_{\mathrm{Cl}}\boldsymbol{r}_{\mathrm{Cl}}$. Choosing the center of mass as the origin, we have $Z_{\mathrm{H}} = \mu/R + m_{\mathrm{H}}/(m_{\mathrm{H}} + m_{\mathrm{Cl}})$. Therefore, the ionic charge evolves according to

$$\frac{d}{dt}Z_{\mathrm{H}}(t) = D\frac{R\frac{d\mu(R)}{dR} - \mu(R)}{R^2}\frac{d}{dt}R(t), \tag{S7}$$

where D is a scaling factor ensuring the correct dissociation limit and $dZ_{\mathrm{Cl}}(t)/dt = -dZ_{\mathrm{H}}(t)/dt$. Note that inclusion of the polarizabilities of the $A^2\Sigma^+$ and $2^2\Sigma^+$ states in the classical simulations does not change our conclusion and thus is omitted for simplicity. When the trajectory moves along different electronic states, the corresponding dipole moment μ is incorporated to account for the charge evolution on the respective state.

From the equations of motion, it is clear that the total momentum of the fragments is constant since $\frac{d^2}{dt^2}(m_{\mathrm{H}}\boldsymbol{r}_{\mathrm{H}} + m_{\mathrm{Cl}}\boldsymbol{r}_{\mathrm{Cl}} + \boldsymbol{r}_{\mathrm{e}}) = 0$ at all instances of time. The conservation of total momentum allows us to leave out the Cl coordinates to simplify the simulation so that only electron and H fragment trajectories are calculated. To initiate the classical simulation, we assume that electron tunneling is instantaneous and preserves the initial internuclear separation and relative nuclear motion, and the electron tunnels

out with vanishing initial velocity antiparallel to the instantaneous electric field at a distance of $R_0/2+I_p/E(t)$ to the geometric center of the molecule, where $R_0 = 2.42$ a.u. is the equilibrium bond length of HCl. The electron and H fragment trajectories are launched with an ionization rate $\Gamma(t) = G(t)W(t)$ in line with MO-ADK [3] and WFAT [5]. Here the field factor is defined as $W(t) = \exp[-2(k_\perp^2 + 2\tilde{I}_p)^{3/2}/3E(t)]$, with $k_\perp$ the initial transverse tunneling momentum of the electron. The structure factor is defined by $G(t) = g_1^2[\Omega(t)]$, with $\Omega(t)$ the angle between the field and molecular orientation directions. The initial conditions for classical dynamics of the electron and hydrogen core in the laser field follow as

$$\begin{cases} \boldsymbol{r}_{\mathrm{e}0} = -\left[\frac{R_0}{2} + \frac{I_p}{E(t)}\right]\frac{\boldsymbol{E}(t)}{E(t)} + \left(\frac{1}{2} - \frac{m_{\mathrm{H}}}{m_{\mathrm{H}}+m_{\mathrm{Cl}}}\right)\boldsymbol{R}_0, \\ \boldsymbol{r}_{\mathrm{H}0} = -\frac{\boldsymbol{r}_{\mathrm{e}0}}{m_{\mathrm{H}}+m_{\mathrm{Cl}}} + \frac{m_{\mathrm{Cl}}}{m_{\mathrm{H}}+m_{\mathrm{Cl}}}\boldsymbol{R}_0, \\ \boldsymbol{k}_{\mathrm{e}0} = \boldsymbol{k}_\perp, \\ \boldsymbol{k}_{\mathrm{H}0} = -\frac{\boldsymbol{k}_\perp}{m_{\mathrm{H}}+m_{\mathrm{Cl}}}. \end{cases} \tag{S8}$$

Last but importantly, an optical-field-induced transient charge of 0.5 is initially placed at the tunneling site if the field vector aligns with the molecular axis. For the case where the field vector forms an angle with the molecular axis, the optical-field-induced transient charge is $0.5\cos^2[\Omega(t)/2]$ at the site near the tunneling exit and $0.5\sin^2[\Omega(t)/2]$ at the site opposite to the tunneling direction. The remaining positive charge of 0.5 is allocated to the composite H−Cl molecular ion. The partitioning of the transient charge into a subcycle optical-field-induced part and a static part is similar to the case of two modes of electron localization with charge-resonance states [12], which sensitively determines subcycle dynamical motion within the system. We note that the use of other initial charge partitioning rather than 0.5 for an optical-field-induced transient charge and the other 0.5 for the composite system will not change the general conclusion of the simulation but lead to worse agreement with the experimental curves.

The most probable dissociation pathway, as shown in Fig. 2(b) of the main text, is to first create a nuclear wave packet on the $A^2\Sigma^+$ state of HCl^+. It afterwards couples to the repulsive $2^2\Sigma^+$ state via three-photon absorption and then couples back to the $A^2\Sigma^+$ via one-photon emission and dissociates into H^+ and Cl fragments with a final momentum around 14 a.u. for each. Granted, the initial excitation to the $A^2\Sigma^+$ state only does not support a subcycle variation of the charge localization, we nonetheless remedy this problem via the introduction of two different modes of charge localization, as specified above. In this way, we could work with the most probable dissociation pathway. Results of the classical simulations, as shown in Figs. 3 and 4 of the main text, are obtained under such considerations.

With the present classical simulations, we can selectively turn off certain interactions to study their influence. If we turn off the Coulomb interaction between the electron and the ions, the rotation angle of the H^+ fragment increases from 2.77° to 3.83°. Therefore, the laser impulse dominates the rotation over the influence of electron-ion interaction. As a result, we focus on the laser impulse in the main text.

[1] H. Akagi, T. Otobe, A. Staudte, A. Shiner, F. Turner, R. Dörner, D. M. Villeneuve, P. B. Corkum, Laser tunnel ionization from multiple orbitals in HCl, Science **325**, 1364 (2009).

[2] L. Xu and F. He, Progress of ultrafast dissociation dynamics for the hydrogen molecule ions, Chin. Sci. Bull. **65**, 4188 (2020).

[3] X.-M. Tong, Z. X. Zhao, and C. D. Lin, Theory of molecular tunneling ionization, Phys. Rev. A **66**, 033402 (2002).

[4] S. F. Zhao, C. Jin, A.-T. Le, T. F. Jiang, and C. D. Lin, Determination of structure parameters in strong-field tunneling ionization theory of molecules, Phys. Rev. A **81**, 033423 (2010).

[5] O. I. Tolstikhin, T. Morishita, and L. B. Madsen, Theory of tunneling ionization of molecules: Weak-field asymptotics including dipole effects, Phys. Rev. A **84**, 053423 (2011).

[6] Q. Sun, T. C. Berkelbach, N. S. Blunt, G. H. Booth, S. Guo, Z. Li, J. Liu, J. McClain, E. R. Sayfutyarova, S. Sharma, S. Wouters, and G. K.-L. Chan, PySCF: the Python-based simulations of chemistry framework, WIREs Comput. Mol. Sci. **8**, e1340 (2018).

[7] J. Wu, L. Ph. H. Schmidt, M. Kunitski, M. Meckel, S. Voss, H. Sann, H. Kim, T. Jahnke, A. Czasch, and R. Dörner, Multiorbital Tunneling Ionization of the CO Molecule, Phys. Rev. Lett. **108**, 183001 (2012).

[8] J. Ma, H. Li, K. Lin, Q. Song, Q. Ji, W. Zhang, H. X. Li, F. Sun, J. Qiang, P. Lu, X. Gong, H. Zeng, and J. Wu, Prompt and delayed Coulomb explosion of doubly ionized hydrogen chloride molecules in intense femtosecond laser fields, Phys. Rev. A **97**, 063407 (2018).

[9] P. Wustelt, F. Oppermann, L. Yue, M. Möller, T. Stöhlker, M. Lein, S. Gräfe, G. G. Paulus, A. M. Sayler, Heteronuclear Limit of Strong-Field Ionization: Fragmentation of HeH + by Intense Ultrashort Laser Pulses, Phys. Rev. Lett., **121**, 073203 (2018).

[10] L. Yue, P. Wustelt, A. M. Sayler, F. Oppermann, M. Lein, G. G. Paulus, and S. Gräfe, Strong-field polarizability-enhanced dissociative ionization, Phys. Rev. A **98**, 043418 (2018).

[11] G. Maroulis, On the dipole polarizability of HCl, Mol. Phys. **74**, 131 (1991).

[12] N. Takemoto and A. Becker, Time-resolved view on charge-resonance-enhanced ionization, Phys. Rev. A **84**, 023401 (2011).